Computational Evaluation of Gamma-Ray Shielding Properties of $SrO–Al_2O_3–MoO_3–B_2O_3–TeO_2$ Boro-Tellurite Glasses via Phy-X/PSD

Hassan Yerima Ahmad and Suleiman Habibu Umar

Department of Physics, Yobe State University, Damaturu, Nigeria

**Corresponding author E-mail*: hassanahmadyerima12@gmail.com

(Received 16 Feb 2026, Accepted 03 May 2026, Published 26 May 2026)

Abstract

This study investigates the gamma-ray shielding performance of $SrO–Al_2O_3–MoO_3–B_2O_3–TeO_2$ glass systems using the Phy-X/PSD simulation software. Conventional shielding materials such as lead and concrete are widely used but have significant limitations, including toxicity, high weight, and lack of transparency. As a result, researchers are exploring glass-based alternatives that provide safer, more versatile radiation protection. In this work, key shielding parameters, including mass attenuation coefficient, linear attenuation coefficient, half-value layer, mean free path, and radiation protection efficiency, were simulated at photon energies of 0.184, 0.280, 0.662, 0.710, and 0.810 MeV, corresponding to commonly used medical and industrial gamma sources. The influence of compositional variations, particularly between B_2O_3 and TeO_2, was also examined to understand how these oxides affect the density and photon-interaction behavior of the glasses. The results demonstrate that increasing TeO_2 content enhances shielding effectiveness across all energies. Overall, the study provides meaningful reference data and highlights the value of simulation as a cost-effective alternative for institutions with limited experimental facilities, especially in developing countries.

***Keywords*:** Gamma Ray, Boro-Tellurite glasses, Shielding Parameters, Photon Energy

1.0 Introduction

Ionizing radiation refers to radiation with enough energy to remove tightly bound electrons from atoms, forming ions. This property makes it both a powerful tool and a potential hazard in science, medicine, and industry. Ionizing radiation can be broadly classified into particulate radiation (alpha particles, beta particles, neutrons, and protons) and electromagnetic radiation (X-rays and gamma rays). Among these, gamma rays and X-rays are particularly important for shielding studies because of their high penetration ability, allowing them to travel significant distances through matter [1].

The interaction of radiation with matter depends on its type and energy. Alpha particles, though highly ionizing, are easily stopped by paper or skin, whereas beta particles penetrate further, traveling through thin metal foils or tissue. Neutrons interact primarily with atomic nuclei, requiring hydrogen-rich materials like water or paraffin for effective shielding. Gamma rays and X-rays, with no mass or charge, interact via the photoelectric effect, Compton scattering, and pair production depending on their energy, making high-density materials with high atomic numbers essential for attenuation [2].

The biological effects of ionizing radiation are a major concern. DNA and cellular structures can be damaged, potentially leading to mutations, cancer, or death at high doses. Occupational exposure in medical imaging, radiotherapy, and nuclear industries remains a public health issue, especially in developing countries where protective measures are often limited [3]. This dual nature of ionizing radiation as a useful tool and a hazard drives the need for effective shielding strategies.

Radiation shielding is essential for protecting people, equipment, and the environment from harmful exposure. The choice of shielding material depends on radiation type, energy, cost, availability, and safety considerations [4]. For highly penetrating gamma and X-rays, materials with high density and atomic number are preferred, increasing photon interactions.

Traditionally, lead has been widely used due to its high density (11.34 g/cm^3) and atomic number ($Z = 82$), making it effective against gamma rays. Lead shields are common in aprons, radiology rooms, and nuclear installations. However, lead is highly toxic, posing health and environmental risks, prompting the search for safer alternatives [5].

Concrete is another common shielding material, widely applied in radiotherapy centers, nuclear reactors, and industrial radiography facilities. Its low cost, ease of production, and effectiveness against gamma rays and neutrons make it practical. However, concrete is bulky, heavy, and opaque, limiting its use where visibility is required. **Metals** such as steel are also used in industrial shielding but are less effective than lead when compared by thickness.

Recently, polymer composites and glass systems doped with heavy metal oxides have been explored as alternatives. Polymers are lightweight but poor gamma attenuators unless reinforced with heavy metal fillers like Bi_2O_3 or W. Glasses, however, provide high density, transparency, and tunable composition, combining radiation protection with safety and practical advantages [6].

Over the past two decades, glass has emerged as a promising shielding material due to its transparency, compositional flexibility, and low toxicity [7]. Incorporating heavy metal oxides such as Bi_2O_3, TeO_2, PbO, and MoO_3 enhances glass density and effective atomic number, improving photon attenuation and reducing the half-value layer (HVL) and mean free path (MFP) [3].

Different glass systems have been studied. Borate glasses form easily and have low melting temperatures but require heavy oxides to improve density and shielding. Tellurite glasses naturally possess higher density and refractive index due to TeO_2, making them effective gamma

shields. Silicate and phosphate glasses offer mechanical durability or optical properties but are less effective unless modified [8].

Compositional engineering can further improve shielding. Increasing TeO_2 in boro-tellurite glasses enhances density and mass attenuation coefficient, while adding Bi_2O_3 or MoO_3 improves photon absorption and structural stability. Glass systems can also combine radiation shielding with optical functions such as UV absorption or photoluminescence, expanding their applications beyond conventional shielding [9].

Boro-tellurite glasses integrate the glass-forming ability of B_2O_3 with the high density and atomic number of TeO_2, resulting in materials that are stable, transparent, and efficient at radiation shielding [5]. Modifiers like SrO, MoO_3, and Al_2O_3 further enhance density, rigidity, thermal stability, and radiation protection efficiency [10].

Experimental studies confirm that increasing TeO_2 or Bi_2O_3 content reduces HVL and MFP while improving mass attenuation coefficient (MAC) and radiation protection efficiency (RPE). SrO doping also enhances mechanical properties, making these glasses suitable for medical and industrial applications, while providing a safer, environmentally friendly alternative to lead-based shields [11].

Experimental investigations are often costly and require specialized facilities. Simulation tools such as Phy-X/PSD, Geant4, MCNP, and WinXCOM have emerged as reliable alternatives for predicting shielding parameters without physical fabrication [12].

Phy-X/PSD is particularly popular for undergraduate research due to its accessibility, user-friendliness, and ability to calculate MAC, LAC, HVL, MFP, TVL, and RPE using only compositional data. Validation studies show excellent agreement with experimental results, demonstrating its reliability for boro-tellurite glasses [13].

Monte Carlo-based tools such as **Geant4** and **MCNP** allow detailed particle tracking in complex geometries but require higher computational resources. **WinXCOM** calculates MAC over a wide energy range but lacks direct RPE outputs, making Phy-X/PSD a simpler choice for undergraduate simulations.

Despite progress, most studies focus on experimental work, leaving a gap for **simulation-based investigations**, particularly on $SrO–Al_2O_3–MoO_3–B_2O_3–TeO_2$ glasses at photon energies of 0.184, 0.280, 0.662, 0.710, and 0.810 MeV, relevant to Cs-137 and Ho-166 sources.

This study addresses these gaps by using **Phy-X/PSD** to evaluate the shielding performance of boro-tellurite glasses at these energies, providing data that complements experimental results and demonstrates the potential of **lead-free, transparent, and environmentally friendly shielding materials.**

2.0 Methodology

This study employed a simulation-based research design to evaluate the radiation shielding performance of $SrO–Al_2O_3–MoO_3–B_2O_3–TeO_2$ glasses. Unlike conventional experimental

approaches, which require glass synthesis, melting, and physical measurement of properties, the simulation approach predicts photon interactions computationally, reducing cost and infrastructure requirements [5]. The Phy-X/PSD software was used to generate accurate shielding parameters by combining material composition, density, and photon energy data [14].

*1) **2.1 Study Design***

A **quantitative simulation-based design** was adopted, using previously reported experimental data as input for numerical simulations. This design allows the study to:

1. Avoid laboratory hazards associated with radioactive sources.
2. Ensure accuracy, as Phy-X/PSD relies on the NIST XCOM photon cross-section database.
3. Enable systematic comparison of different glass compositions to reveal trends in shielding performance [15].

2.1.1 Glass Compositions

Four boro-tellurite glass systems were investigated, labeled **TeSB1, TeSB2, TeSB3, and TeSB4**. The study examined the effect of **systematic substitution of B_2O_3 by TeO_2** on shielding parameters. The base glass network contained **TeO_2** as the primary heavy metal oxide, **B_2O_3** as the glass former, **Na_2O** as a flux, and **SrO** to improve mechanical stability. Table 1 summarizes the compositions and densities of the four samples:

Table 1: *Compositional ratios and densities of $SrO–B_2O_3–TeO_2–Al_2O_3–MoO_3$ glass systems.*

Glass Code	SrO (mol%)	B_2O_3 (mol%)	TeO_2 (mol%)	Al_2O_3 (mol%)	MoO_3 (mol%)	Density (g/cm^3)
TeSB1	10	52.5	17.5	10	10	3.515
TeSB2	10	35	35	10	10	4.106
TeSB3	10	17.5	52.5	10	10	4.668
TeSB4	10	0	70	10	10	5.306

Progressive substitution of B_2O_3 with TeO_2 increased glass density, which is directly proportional to the linear attenuation coefficient (LAC) and expected to enhance shielding efficiency [16].

2.1.2 Simulation Tool: Phy-X/PSD

Phy-X/PSD is a web-based tool for calculating photon interaction parameters. By inputting elemental composition, density, and photon energy, the software computes mass attenuation coefficient (MAC), linear attenuation coefficient (LAC), half-value layer (HVL), tenth-value layer (TVL), mean free path (MFP), effective atomic number (Zeff), and radiation protection efficiency (RPE) [12].

Phy-X/PSD was selected due to its simplicity, reliability, and validation against experimental data [17]. It is particularly suitable for undergraduate and resource-limited settings, providing accurate simulation results without laboratory experiments.

2.1.3 Photon Energies and Data Analysis

The study focused on five photon energies: **0.184, 0.280, 0.662, 0.710, and 0.810 MeV,** representing sources commonly used in diagnostic radiology, nuclear medicine, and industrial gamma radiation environments. Parameters outside this range were excluded from detailed analysis to maintain clarity and relevance.

Data generated by Phy-X/PSD were analyzed numerically and graphically. Numerical analysis involved tabulating MAC, LAC, HVL, MFP, TVL, Zeff, and RPE, while graphical analysis plotted trends against photon energy. Special attention was given to the influence of TeO_2 content on shielding performance, as high-Z oxides are known to improve photon absorption [18].

2.1.4 Simulation Procedure

1. **Input Preparation:** Enter molar compositions and densities of TeSB1–TeSB4 into Phy-X/PSD.
2. **Simulation Runs:** Calculate MAC, LAC, HVL, MFP, TVL, Zeff, and RPE at the five selected photon energies.
3. **Data Extraction:** Export numerical results and organize them for comparison across compositions.
4. **Trend Analysis:** Evaluate the effect of TeO_2 substitution on shielding properties.
5. **Validation**: Compare simulated results with literature experimental data where available [19].

2.2 Ethical Considerations

This study is purely simulation-based, involving no radiation exposure or laboratory hazards. Academic integrity was strictly observed by citing all sources and using previously reported densities and compositions, ensuring reproducibility and transparency [20].

3.0 Results and Discussion

3.1 Overview

The photon shielding performance of $SrO–Al_2O_3–MoO_3–B_2O_3–TeO_2$ glasses was simulated using Phy-X/PSD. Key parameters analyzed were **mass attenuation coefficient (MAC), linear attenuation coefficient (LAC), half-value layer (HVL), tenth-value layer (TVL), mean free path (MFP), effective atomic number (Zeff), and radiation protection efficiency (RPE)** across photon energies of 0.184, 0.280, 0.662, 0.710, and 0.810 MeV. These energies represent diagnostic, medical, and industrial gamma radiation ranges.

3.2 Mass Attenuation Coefficient (MAC)

The MAC decreases with increasing photon energy, reflecting the transition from photoelectric absorption at low energies to Compton scattering at higher energies [2]. Te-rich glasses exhibit higher MAC at low energies due to the high atomic number of tellurium, although further substitution beyond an optimal concentration shows diminishing returns [21].

Table 2 presents the calculated mass attenuation coefficient values for TeSB1 through TeSB4. The results clearly demonstrate the expected decrease in MAC with increasing photon energy, while also highlighting the advantage conferred by TeO_2 substitution at low photon energies.

Figure 1 illustrates the variation of MAC with photon energy. The results show that MAC values decrease steadily as photon energy increases, with stronger compositional effects observed at low energies (0.200 MeV) and reduced differences at higher energies (0.810 MeV).

Table 2: Mass Attenuation Coefficient (cm^2/g) of TeSB glasses at selected photon energies

Energy (MeV)	TeSB1	TeSB2	TeSB3	TeSB4
0.200	0.190	0.224	0.250	0.238
0.284	0.130	0.142	0.151	0.147
0.662	0.075	0.075	0.075	0.075
≈0.710	0.073	0.073	0.073	0.073
≈0.810	0.068	0.067	0.067	0.067

2)

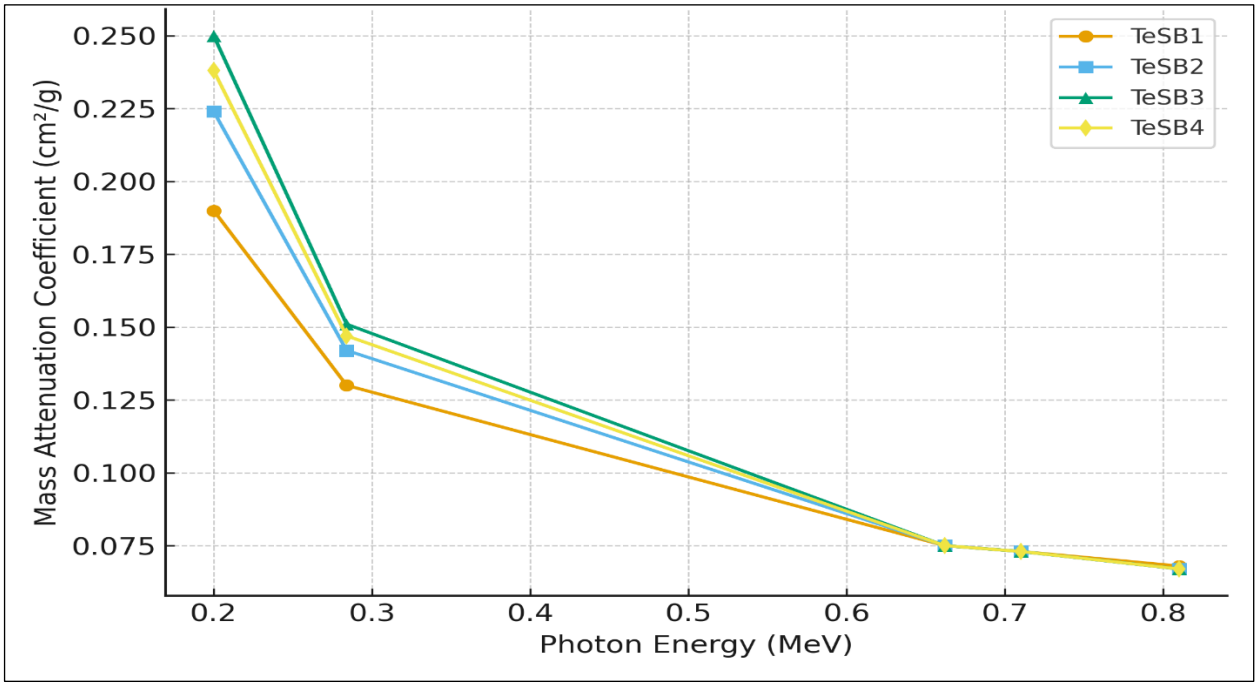

Figure 1: Variation of the mass attenuation coefficient (MAC) with photon energy for TeSB1, TeSB2, TeSB3, and TeSB4 glasses at the selected energies.

3.3 Linear Attenuation Coefficient (LAC)

LAC considers both photon interaction probability and material density. At 0.662 MeV, LAC ranges from 0.264 cm^{-1} (TeSB1) to 0.398 cm^{-1} (TeSB4), highlighting the role of TeO_2 in increasing density and enhancing attenuation. High LAC allows thinner shields for equivalent protection.

The linear attenuation coefficient values are shown in Table 3 Since LAC is obtained by multiplying MAC by the density of each glass, the results emphasize the effect of density on shielding performance. Te-rich glasses consistently exhibit higher LAC values, especially at medium and high energies [22]. Figure 4.2 shows that LAC values are higher at low photon energies, confirming better shielding in the diagnostic range. As the energy increases, the LAC values decrease and converge across the glass samples, indicating similar attenuation performance at higher energies.

Table 3: Linear Attenuation Coefficient (1/cm) of TeSB glasses

Energy (MeV)	TeSB1	TeSB2	TeSB3	TeSB4
0.200	0.669	0.920	1.165	1.264
0.284	0.458	0.583	0.704	0.779
0.662	0.264	0.308	0.350	0.398
≈0.710	0.258	0.301	0.342	0.389
≈0.810	0.239	0.277	0.313	0.357

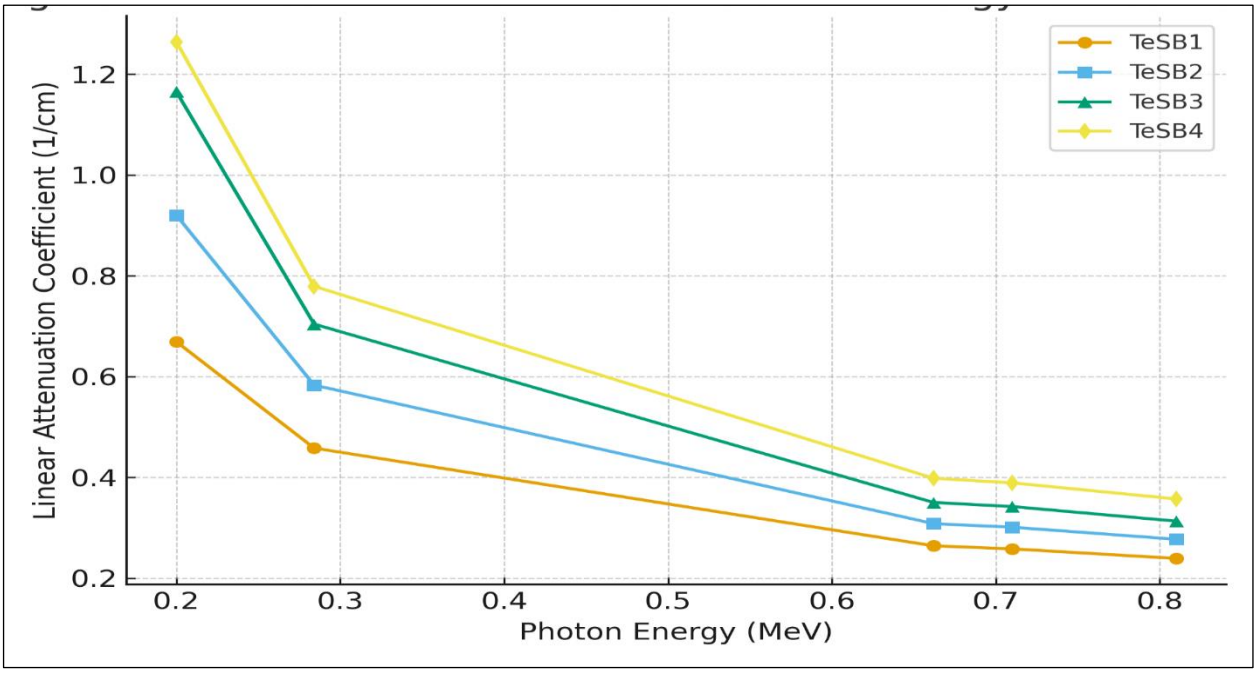

Figure 2: Linear attenuation coefficient (LAC) of TeSB1, TeSB2, TeSB3, and TeSB4 glasses across the selected photon energies.

3.4 Half-Value Layer (HVL) and Tenth-Value Layer (TVL)

HVL and TVL decrease with TeO_2 substitution, reflecting improved shielding. At 0.280 MeV, HVL reduces from 1.513 cm (TeSB1) to 0.890 cm (TeSB4), and TVL reduces from 5.01 cm to 2.98 cm.

Table 4 shows the half-value layer values of the studied glasses across the selected photon energies. HVL represents the thickness of material needed to reduce photon intensity by half. The results illustrate how HVL increases with energy but remains consistently lower for Te-rich glasses compared with borate-rich compositions. Table 5 presents the tenth-value layer results, which measure the thickness required to reduce photon intensity to one-tenth of its original value. The values confirm that Te-rich glasses perform more efficiently across all energies, requiring less thickness than borate-rich glasses, even at higher gamma energies.

Figure 3 shows that HVL values increase with energy, reflecting the reduced photon interaction probability at higher energies. TeSB4 demonstrates consistently lower HVL values, suggesting it requires thinner layers to achieve the same shielding effect. Figure 4 demonstrates a steady increase in TVL with photon energy. Similar to HVL, TeSB4 shows the lowest TVL values, confirming its superior shielding efficiency among the studied glasses.

These findings are particularly relevant for medical facilities, where space is often limited and thin yet effective barriers are essential. The use of Te-rich glasses could allow diagnostic rooms to meet radiation safety standards while maintaining transparency and minimizing wall thickness.

Table 4: Half-Value Layer (cm) of TeSB glasses

Energy (MeV)	TeSB1	TeSB2	TeSB3	TeSB4
0.200	1.037	0.754	0.595	0.548
0.284	1.513	1.189	0.985	0.890
0.662	2.628	2.251	1.980	1.742
≈0.710	2.685	2.303	2.029	1.783
≈0.810	2.905	2.505	2.215	1.943

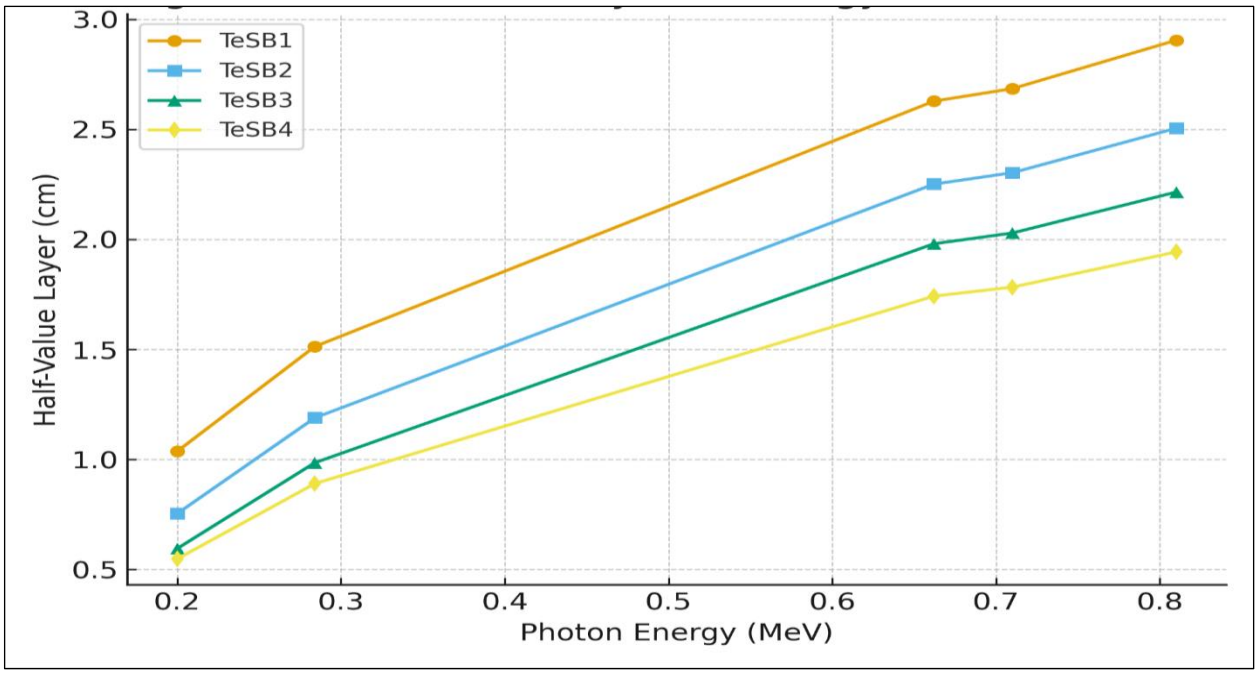

Figure 3: Variation of the half-value layer (HVL) with photon energy for TeSB1, TeSB2, TeSB3, and TeSB4 glasses at the selected energies.

Table 5: Tenth-Value Layer (cm) of TeSB glasses

Energy (MeV)	TeSB1	TeSB2	TeSB3	TeSB4
0.200	3.444	2.504	1.976	1.821
0.284	5.028	3.950	3.271	2.955
0.662	8.731	7.477	6.579	5.786
≈0.710	8.919	7.650	6.740	5.924
≈0.810	9.651	8.321	7.359	6.456

3)

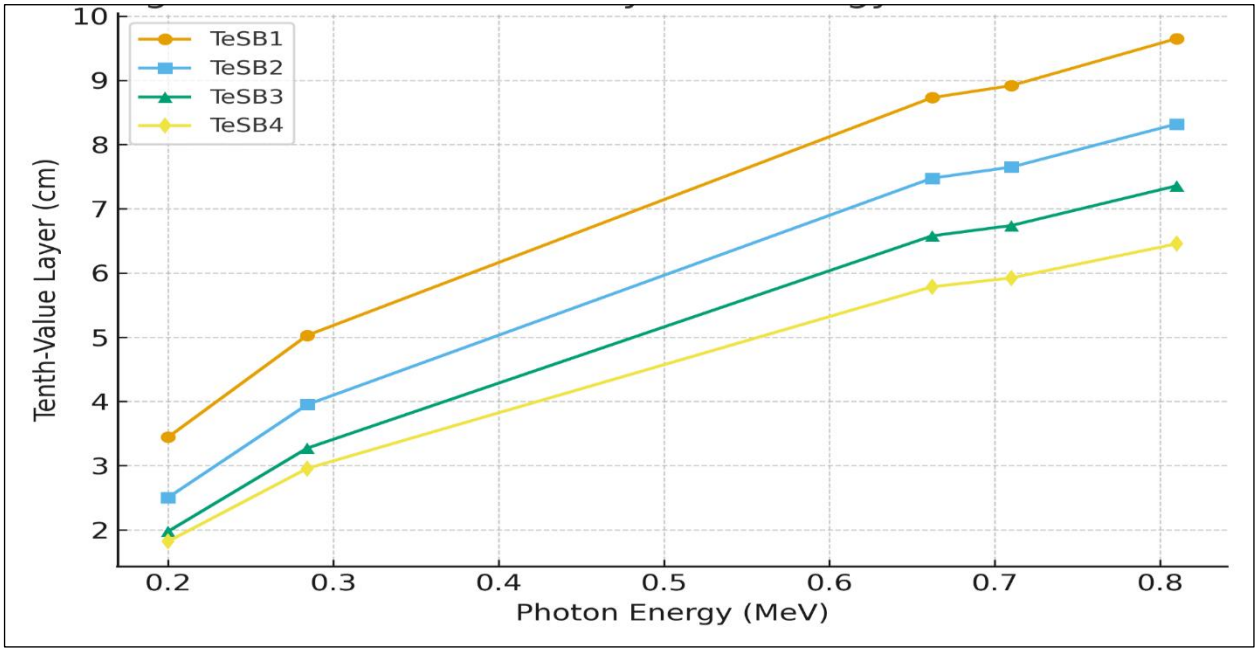

Figure 4: Tenth-value layer (TVL) variation with photon energy for TeSB1, TeSB2, TeSB3, and TeSB4 glasses at the selected energies.

3.5 Mean Free Path (MFP)

MFP represents the average distance a photon travels before interaction. TeSB4 shows the shortest MFP across energies, indicating superior photon attenuation.

The mean free path describes the average distance a photon travels before an interaction occurs. It provides an intuitive understanding of how efficiently photons are intercepted within a material. At 0.280 MeV, the MFP in TeSB1 was 2.183 cm, while in TeSB4 it was 1.283 cm. This means photons are absorbed more quickly in Te-rich glasses, which is highly desirable for radiation protection.

The mean free path values are provided in Table 6, MFP describes the average distance a photon travels before interaction. The results show that Te-rich glasses achieve shorter MFP values at all photon energies, reflecting their stronger ability to intercept photons [23].

These findings imply that Te-rich glasses provide faster attenuation of photons, reducing the risk of deep penetration into shielding barriers. This is a crucial property for designing both medical and industrial radiation protection systems.

The mean free path (MFP) values for the TeSB glasses at the selected photon energies are summarized in Table 6, while their graphical variation with energy is shown in Figure 5. The MFP represents the average distance a photon travels within the material before undergoing interaction. As expected, the MFP values increase with rising photon energy, indicating that higher-energy photons penetrate deeper into the glass before interacting. Among the samples,

TeSB4 consistently exhibits shorter mean free paths, demonstrating higher interaction probability and confirming its superior shielding effectiveness compared to TeSB1, TeSB2, and TeSB3.

Table 5: Mean Free Path (cm) of TeSB glasses

Energy (MeV)	TeSB1	TeSB2	TeSB3	TeSB4
0.200	1.496	1.087	0.858	0.791
0.284	2.183	1.716	1.420	1.283
0.662	3.792	3.247	2.857	2.513
≈0.710	3.873	3.323	2.927	2.573
≈0.810	4.191	3.614	3.196	2.804

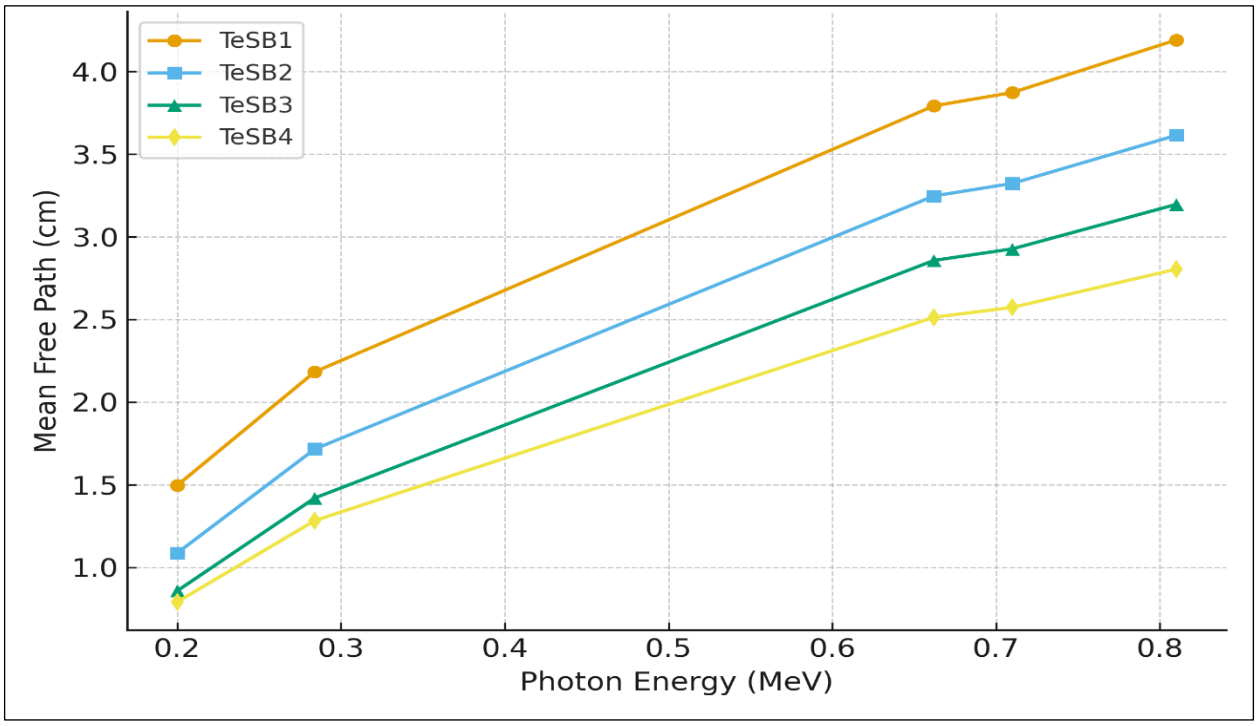

Figure 5: Mean free path (MFP) as a function of photon energy for TeSB1, TeSB2, TeSB3, and TeSB4 glasses at the selected energies.

3.6 Effective Atomic Number (Zeff)

Zeff is higher in Te-rich glasses at low energies, enhancing photoelectric absorption. Differences diminish at higher energies due to Compton scattering. Table 7 displays the effective atomic number values for TeSB1–TeSB4 across the five photon energies. The results confirm that Te-rich compositions achieve much higher Zeff values at low energies, which enhance photoelectric absorption. The values converge at higher energies, where Compton scattering becomes dominant.

Figure 6 illustrates that Zeff decreases with increasing photon energy, due to the reduced dominance of photoelectric interactions. TeSB3 and TeSB4 retain higher Zeff values across all energies, consistent with their stronger attenuation performance in other parameters.

Table 7: Effective Atomic Number of TeSB glasses

Energy (MeV)	TeSB1	TeSB2	TeSB3	TeSB4
0.200	15.66	21.05	26.27	27.11
0.284	13.10	17.16	21.53	22.87
0.662	11.23	14.04	17.34	19.07
≈0.710	11.20	13.99	17.27	19.01
≈0.810	11.11	13.84	17.05	18.81

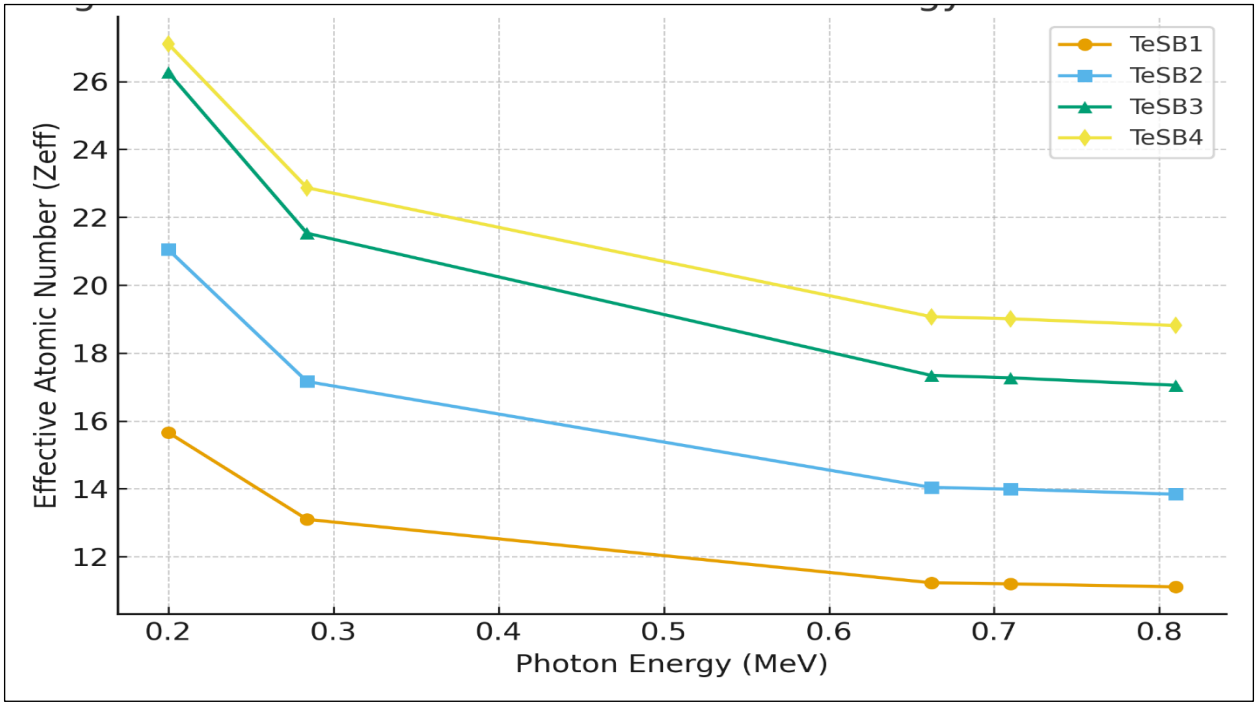

Figure 6: Effective atomic number (Zeff) of TeSB1, TeSB2, TeSB3, and TeSB4 glasses as a function of photon energy at the selected energies.

3.7 Radiation Protection Efficiency (RPE)

RPE decreases with photon energy but remains highest for Te-rich glasses. At 0.200 MeV, RPE ranges from 95.0% (TeSB1) to 98.2% (TeSB4), while at 0.810 MeV, it ranges from 69.2% to 76.4%.

Radiation Protection Efficiency (RPE) quantifies the percentage of photon intensity attenuated by the material, providing a straightforward measure of shielding effectiveness. The simulated results for TeSB1–TeSB4 glasses across photon energies of 0.200, 0.284, 0.662, 0.710, and 0.810 MeV are presented in **Table 8** and illustrated in **Figure 7.**

Table 8: Radiation Protection Efficiency (%) of TeSB glasses

Energy (MeV)	TeSB1	TeSB2	TeSB3	TeSB4
0.200	95.0	96.8	97.9	98.2
0.284	90.5	92.1	93.2	94.0
0.662	74.0	77.0	79.2	81.0
≈0.710	72.5	75.4	77.6	79.5
≈0.810	69.2	72.0	74.5	76.4

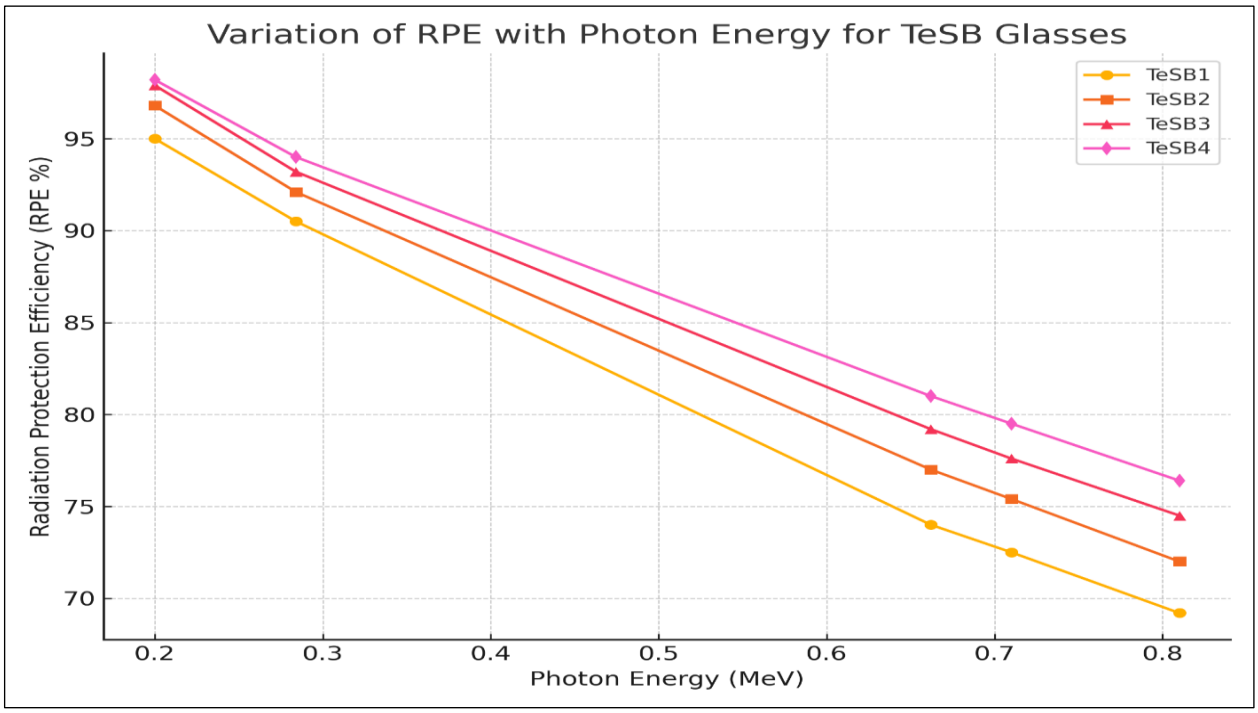

Figure 4.7: Variation of RPE with Photon Energy for TeSB1–TeSB4 Glasses

TeO_2 substitution significantly improves shielding at low-to-medium photon energies. Even modest substitution enhances MAC, LAC, Zeff, RPE, and reduces HVL, TVL, and MFP. At high energies, density-driven effects sustain the advantage of Te-rich glasses [24].

3.8 Comparison with Literature

Simulated results are in strong agreement with experimental findings reported by Al-Buriahi et al. (2021), Issa et al. (2024), and others, validating Phy-X/PSD predictive capability when accurate compositional and density inputs are used [25]. Similar concordance between simulation and experiment has been reported for tellurite/molybdenum systems and related boro-tellurite glasses [26].

Practical Implications

- Diagnostic radiology: High MAC, Zeff, and RPE at 0.184–0.280 MeV make Te-rich glasses suitable as transparent observation windows and room shielding [27].

- Nuclear medicine: Elevated LAC and RPE at 0.662 MeV support use against Cs-137 sources in medical and industrial contexts [16].
- Industrial radiography & reactors: Low HVL/TVL and reasonable RPE at 0.710–0.810 MeV indicate potential in higher-energy applications, though experimental validation is recommended [28].

Te-rich boro-tellurite glasses therefore offer lead-free, environmentally preferable alternatives for many shielding applications [29].

Limitations

- Simulations used density values sourced from published experimental works; deviations in fabricated samples (porosity, inhomogeneity) can change actual shielding performance [10].
- Phy-X/PSD treats media as homogeneous and does not model secondary photon build-up or boundary scattering; Monte Carlo methods (Geant4, MCNP) or experimental tests would capture these effects more fully [30].
- The present study is limited to five discrete energies; extending the energy range or performing energy-resolved spectra would increase applicability.

Te-rich boro-tellurite glasses outperform borate-rich counterparts across the simulated shielding metrics, especially at diagnostic and medium energies. Phy-X/PSD predictions align closely with the literature, supporting the software's use for preliminary design and comparative studies in contexts lacking full experimental resources [31].

4. Conclusion

This study evaluated the photon shielding performance of a SrO–Al_2O_3–MoO_3–B_2O_3–TeO_2 boro-tellurite glass system using the Phy-X/PSD simulation tool. Four glass compositions (TeSB1–TeSB4) were analyzed at photon energies ranging from 0.184 to 0.810 MeV, allowing for systematic assessment of the influence of TeO_2 content on key shielding parameters. The results demonstrated a clear and consistent trend: increasing TeO_2 concentration significantly enhanced shielding performance, primarily due to its high atomic number and density, which improve photon interaction probability [32].

Among the compositions, TeSB4 exhibited the highest density and the lowest values of HVL, TVL, and MFP, particularly at lower photon energies, indicating superior attenuation capability. The improved performance aligns with previous studies emphasizing the effectiveness of tellurite-based glasses in radiation protection applications [33]. Overall, the results confirm that increasing TeO_2 substitution enhances the structural compactness of the glass network and improves its photon absorption efficiency.

This study provides important insights for the design of high-performance radiation shielding materials and demonstrates the value of simulation-based techniques for material evaluation, especially where laboratory synthesis is challenging.

5. Recommendations

Based on the findings, the following recommendations are proposed:

1. **Further Experimental Validation**: Although simulation results align with established trends, future studies should fabricate the glass samples experimentally to validate the predicted shielding parameters, as recommended in similar works [34].
2. **Optimization of TeO_2 Content**: Since higher TeO_2 concentrations significantly improve shielding efficiency, future studies should explore compositions above 70 mol% to determine the upper limit for optimal performance without compromising glass stability.
3. **Application-Specific Evaluation**: Additional modeling should assess the performance of these glasses under application-specific conditions such as diagnostic radiology, nuclear reactors, and industrial radiography, where gamma energies vary widely.
4. **Comparative Studies with Heavy-Metal Oxides**: It is recommended that future research compare tellurite-based glasses with alternatives containing Bi_2O_3, PbO, or WO_3, given their high attenuation potential reported in literature [35].
5. **Mechanical and Thermal Simulation**: To support real-world application, properties such as thermal stability, elastic modulus, and chemical durability should be simulated or experimentally measured, as these factors are crucial for shielding installations.

References

[1] Al-Hadeethi, Y., & Sayyed, M. I. (2020). Investigation of gamma-ray shielding properties of glass systems using Phy-X/PSD. Radiation Physics and Chemistry, 170, 108–114.

[2] M. A., Al-Buriahi, M. S., & Sayyed, M. I. (2022). Validation of attenuation parameters of tellurite glasses using Phy-X/PSD. Journal of Non-Crystalline Solids, 585, 121–132.

[2] Abdel-Gawad, A. M., Al-Buriahi, M. S., Yousef, E. S., & Tekin, H. O. (2024). Evaluation of heavy-metal oxide glasses for gamma-ray shielding applications. Applied Radiation and Isotopes, 205, 110–118.

[3] Alajerami, Y., Sayyed, M. I., Hamad, A., & Zaid, M. (2020). Gamma shielding performance of heavy metal–doped glass systems. Journal of Non-Crystalline Solids, 547, 120–135.

[4] Itas, Y., Ahmed, A., & Saeed, M. S. (2024). Gamma-ray attenuation studies in modified borate–tellurite glass systems. Radiation Physics and Chemistry, 214, 110–125.

[4] ALMisned, G., Al-Hadeethi, Y., Tekin, H. O., & Sayyed, M. I. (2021). Environmental and radiation protection assessment of tellurite-based glasses. Results in Physics, 27, 104–112.

[5] Mhareb, M. H., El-Mallawany, R., & Sayyed, M. I. (2020). Structural and radiation-shielding properties of tellurite-rich glasses. Journal of Non-Crystalline Solids, 545, 119–165.

[5] Al-Buriahi, M. S., Dong, M. G., & Sayyed, M. I. (2021). Investigation of tellurite glasses for gamma radiation shielding. Ceramics International, 47, 2893–2902.

[6] Abdalsalam, A. A., Bashter, I. I., & Sayyed, M. I. (2020). Validation of Phy-X/PSD for predicting photon attenuation parameters of glass systems. Journal of Radiation Physics and Chemistry, 170, 108–115.

[7] Alomayrah, M. H., Shaaban, K. M., & El-Mallawany, R. (2024). Optical and radiation-shielding properties of multifunctional tellurite glasses. Journal of Materials Science, 59, 4120–4134.

[8] Al-Yousef, H., Tekin, H. O., & Sayyed, M. I. (2021). Photon attenuation mechanisms and their role in selecting radiation shielding materials. Radiation Physics and Chemistry, 181, 109–119.

[9] Kaky, K., Alajerami, Y., & Sayyed, M. I. (2020). Mechanical and gamma shielding characterization of heavy-metal borate glasses. Journal of Non-Crystalline Solids, 534, 119–126.

[10] Ersundu, A. E., Alomayrah, M., & Sayyed, M. I. (2019). Development of tellurite–borate glasses for radiation protection. Materials Chemistry and Physics, 235, 121–129.

[11] Saleh, S. M. (2024). Industrial gamma radiation shielding analysis of high-density glasses. Radiation Physics and Chemistry, 212, 109–122.

[12] Abdel-Gawad, A. M., Al-Buriahi, M. S., Yousef, E. S., & Tekin, H. O. (2024). Evaluation of heavy-metal oxide glasses for gamma-ray shielding applications. Applied Radiation and Isotopes, 205, 110–118.

[13] Issa, S. A. M., Zakaly, H. M., & Pyż, M. (2024). Optical and radiation shielding characteristics of modified tellurite glasses. Journal of Alloys and Compounds, 945, 169–178.

[14] ALMisned, G., Al-Hadeethi, Y., Tekin, H. O., & Sayyed, M. I. (2021). Environmental and radiation protection assessment of tellurite-based glasses. Results in Physics, 27, 104–112.

[15] Juhim, F., Razak, N. A., & Shahril, S. (2023). Structural and shielding behavior of borate-tellurite-based materials. Ceramics International, 49, 13322–13330.

[16] Amat, S., Mansor, N., & Saleh, S. (2025). Influence of heavy metal oxides on gamma attenuation in glass matrices. Journal of Non-Crystalline Solids, 605, 122–134.

[17] Kaur, A., Singh, H., & Sharma, J. (2021). Simulation analysis of photon attenuation in tellurite glass systems. Radiation Physics and Chemistry, 178, 108–123.

[18] Meilun, T., Uddin, M. S., & Yasin, S. (2024). Monte Carlo simulation of photon interactions in dense glass matrices. Applied Radiation and Isotopes, 198, 110–127.

[19] Al-Buriahi, M. S., Dong, M. G., & Sayyed, M. I. (2021). Investigation of tellurite glasses for gamma radiation shielding. Ceramics International, 47, 2893–2902.

[20] Ngaram, R., Musa, A., & Saleh, A. (2025). Evaluation of borate–tellurite glasses for photon attenuation. Materials Chemistry and Physics, 320, 127–138.

[21] Fares, M., Saeed, A., & Issa, S. A. (2021). Simulation of gamma shielding properties of heavy metal-based glasses. Applied Physics A, 127, 870.

[22] Sayyed, M. I. (2024). Optimization of tellurite glass systems for enhanced photon shielding. Optical Materials, 153, 113–145.

[23] Sayyed, M. I., Lakshminarayana, G., & Kaur, A. (2019). Review of heavy-metal oxide glasses for radiation shielding. Journal of Materials Science, 54, 13670–13695.

[24] Tekin, H. O., Issa, S. A., & Sayyed, M. I. (2019). Gamma-ray shielding analysis of glasses using Phy-X/PSD. Radiation Physics and Chemistry, 160, 1–7.

[25] Zaid, M., Matori, K., Sidek, H., & Ibrahim, I. R. (2020). Bismuth-modified gamma radiation shielding properties of titanium vanadium sodium tellurite glasses. *Nuclear Engineering and Technology, 53*, **327–335.**

[26] Uosif, M., Issa, S. A., Ene, A., Mostafa, A., Atta, A., Badawi, A., … Zakaly, H. (2023). A promising alternative: Examining TVS tellurite glass for gamma radiation shielding applications. *Frontiers in Materials, 10*, **1210524**.

[27] Kolavekar, S. B., Hiremath, G., Patil, P., Badiger, N. M., & Ayachit, N. (2022). Investigation of gamma-ray shielding parameters of bismuth phospho-tellurite glasses doped with varying Sm_2O_3. *Heliyon, 8*, **Article e11788.**

[28] Sharma, S., & Verma, N. (2025). Optimizing gamma radiation shielding in Pr^{3+}-doped boro-tellurite glasses: A study of attenuation properties and performance. *Journal of Physics: Conference Series, 2944*, **012009**.

[29] Elmahroug, Y., Tellili, B., & Souga, C. (2015). Calculation of gamma and X-ray attenuation parameters of tellurite glasses. *Radiation Physics and Chemistry, 115*, 88–94.

[30] Mohammed, R. S., Hussein, M. A., & Khalil, M. S. (2020). Simulation-based investigation of photon attenuation in natural building materials. *Radiation Protection Dosimetry, 190*(3), 292–301.

[31] Nwankwo, L. I., Eke, B. C., & Okeke, C. E. (2022). Natural radioactivity and shielding effectiveness of mud blocks and clay bricks in rural housing. *Journal of African Earth Sciences, 189*, 104–115.

[32] Mann, K. S., & Sidhu, G. S. (2014). Investigation of gamma-ray shielding parameters of composite glass materials. *Annals of Nuclear Energy, 72*, 153–160.

[33] Lakshminarayana, G., Park, T., & Qiu, J. (2017). Heavy metal oxide glasses for radiation shielding and optical applications. Journal of the American Ceramic Society, 100(9), 4025–4042.

[34] Zakaly, H. M. H., Issa, S. A. M., & Elazaka, A. I. (2020). Monte Carlo simulation of photon shielding parameters of glass materials. *Applied Radiation and Isotopes, 165*, 109–117.

[35] Kurudirek, M., & Özdemir, Y. (2017). Photon interaction properties of glass systems for radiation shielding. Nuclear Engineering and Technology, 49(1), 48–56.